Separation and Purification Technology 282 (2022) 119981

Contents lists available at ScienceDirect

Separation and Purification Technology

journal homepage: www.elsevier.com/locate/seppur

Functionalized polyamide membranes yield suppression of biofilm and planktonic bacteria while retaining flux and selectivity

Mostafa Dadashi Firouzjaei [a,1], Mehdi Pejman [b,1], Mohammad Sharifian Gh [c], Sadegh Aghapour Aktij [d,e], Ehsan Zolghadr [a,f], Ahmad Rahimpour [d,*], Mohtada Sadrzadeh [d], Ahmad Arabi Shamsabadi [g], Alberto Tiraferri [b,*], Mark Elliott [a,*]

[a] Department of Civil, Environmental and Construction Engineering, University of Alabama, Tuscaloosa, AL 35487, United States
[b] Department of Environment, Land and Infrastructure Engineering (DIATI), Politecnico di Torino, Corso Duca degli Abruzzi 24, 10129 Turin, Italy
[c] Department of Cell Biology, University of Virginia, Charlottesville, VA 22908, United States
[d] Department of Mechanical Engineering, 10-367 Donadeo Innovation Center for Engineering, Advanced Water Research Lab (AWRL), University of Alberta, Edmonton, AB T6G 1H9, Canada
[e] Department of Chemical & Materials Engineering, University of Alberta, Edmonton, AB T6G 1H9, Canada
[f] Department of Physics and Astronomy, University of Alabama, Tuscaloosa, AL 35487, United States
[g] Department of Chemistry, University of Pennsylvania, Philadelphia, PA 19104, United States

ARTICLE INFO

Keywords:
Biofilm inhibition
Desalination
Water treatment
Metal azolate framework
Antibacterial membranes
Metal organic framework
MOF
Fouling

ABSTRACT

Biofouling is a major challenge for desalination, water treatment, and water reuse applications using polymer-based membranes. Two classes of novel silver-based metal azolate frameworks (MAF) are proposed to decorate polyamide (PA) forward osmosis membranes and to improve numerous aspects of fouling and transport. Membranes functionalized with two concentrations of each MAF are compared with a pristine control material, with results that clearly highlight their tunability and bio-inhibitory effects. We report for the first time PA membranes yielding near complete suppression of a robust biofilm-forming bacterium (*Pseudomonas aeruginosa*) and inactivation of planktonic bacteria, while maintaining high selectivity. These features improve the long-term water flux performance of the membranes, tested during 24 h of accelerated biofouling and organic fouling conditions, and showing lower than 10% and 20% decline in water flux. These enhancements were achieved with only 0.03–0.06% mass of additives and little generation of hazardous waste products, indicating that low-cost and environmentally benign functionalization can prevent biofouling growth while maintaining selectivity and transport for high-performance desalination, water treatment and reuse.

1. Introduction

Biofilms are ensembles of microorganisms that develop upon attachment to surfaces and that possess biochemical properties, phenotypic characteristics, and architectures distinct from their planktonic and free-swimming counterparts [1]. One of the most important characteristics of biofilms is their antibiotic resistance, which can be up to 1,000-times greater than that of common planktonic cells [2]. This specific property of biofilms is a major challenge for numerous industrial and medical fields [3]. *Pseudomonas aeruginosa* (*P. aeruginosa*) is one such highly-resistant, biofilm-forming bacterial species [4] and is one of the twelve priority pathogens listed by WHO [5]. What further hinders the successful inhibition of this bacterium is that through formation of biofilms, the resistance of *P. aeruginosa* is increased by a self-made protector environment against treatments and host immune defense [6]. There are many studies aimed at mitigating *P. aeruginosa* biofilm formation, but not much success in fully preventing the growth of these communities [7]. Moreover, most of the approaches are not sufficiently

* Corresponding authors at: Department of Civil, Environmental and Construction Engineering, University of Alabama, Tuscaloosa, AL 35487, United States (M. Elliott). Department of Environment, Land and Infrastructure Engineering (DIATI), Politecnico di Torino, Corso Duca degli Abruzzi 24, 10129 Turin, Italy (A. Tiraferri). Department of Mechanical Engineering, Donadeo Innovation Center for Engineering, Advanced Water Research Lab (AWRL), University of Alberta, Edmonton, ABT6G 1H9, Canada (A. Rahimpour).
E-mail addresses: arahimpo@ualberta.ca (A. Rahimpour), alberto.tiraferri@polito.it (A. Tiraferri), melliott@eng.ua.edu (M. Elliott).
[1] The authors contributed equally to this work.

https://doi.org/10.1016/j.seppur.2021.119981
Received 20 August 2021; Received in revised form 4 October 2021; Accepted 17 October 2021
Available online 28 October 2021

reproducible, lack technical validity, or both [8].

Microorganisms are ubiquitous in the environment; controlling or preventing the colonization of surfaces and the growth of biofilms are major challenges for many industries, including those engaged in healthcare, food production, and water treatment [9]. In particular, biofouling has been called the "Achilles' Heel" of membrane-based water treatment [10], causing numerous adverse effects including compromised membrane integrity, resistance to water flux, and deterioration of water quality [11–12]. Control of biofilm formation and removal of existing biofilms are often attempted using remedial actions, such as scouring or disinfection [13]. Unfortunately, polymer-based membranes provide a hospitable environment for biofilm formation, especially when treating nutrient-rich waters [14], and they can be easily damaged by the oxidants commonly used to control biofilm growth [15]. Altering the surface properties of the membrane by increasing hydrophilicity, reducing roughness, and imparting negative surface charge can reduce bacterial attachment and growth [11]. Additionally, incorporation of antimicrobial agents into the membrane surface layer has shown particular promise in mitigating the initial establishment and subsequent growth of biofilms [16–18].

Recent studies have demonstrated some success in controlling biofilm growth and improving water flux through functionalization of membrane surfaces with antimicrobial metal–organic frameworks [17,19–20]. However, most of these studies have shown only moderate improvements in bacterial inactivation, suppression of biofilm, and maintenance of water flux [17,19–20]. Additionally, these studies typically investigated bacteria that do not tend to form robust biofilms, for example, *Escherichia coli* (*E. coli*) [63].

In this study, we fabricated novel thin-film nanocomposite (TFN) polyamide (PA) membranes decorated with silver-based metal-azolate framework (MAF) nanoparticles (NPs). We tested two different organic linkers of the MAF crystals, namely, 2-methylimidazole and benzimidazole, both of which are hypothesized to be seamlessly incorporated within the PA matrix. Both linkers also possess antimicrobial properties of their own, thus potentially increasing the antimicrobial properties of the MAFs [21–22]. We engineered the polyamide surface following the principle of atom economy, thus maximizing the density of MAF starting from dispersion with NP concentrations of only 0.03 and 0.06 wt%. Low concentration of additives reduces cost and increases the feasibility of commercial application.

While a number of approaches to incorporate antimicrobial agents have been successful in partially controlling biofouling and flux reduction, our objective is to provide the first demonstration of all of the following features simultaneously: (i) inactivation of planktonic bacteria, (ii) nearly complete suppression of the growth of a relevant and robust biofilm-forming organism (*P. aeruginosa*), and (iii) retention of flux under simulation of long-term organic fouling and biofouling with a high degree of selectivity. Additionally, this membrane functionalization is achievable through a facile process with low-concentration additives, making this process potentially scalable.

2. Methods

2.1. Materials and Chemicals

Poly (ether sulfone) (PES, M_w of 58,000 g/mol) was purchased from BASF, Germany. Poly (vinylpyrrolidone) (PVP M_w of 25,000 g/mol), N, N-dimethylformamide (DMF), 1,3-phenylenediamine (MPD), n-hexane, trimesoyl chloride (TMC), sodium chloride (NaCl), silver nitrate ($AgNO_3$), benzimidazole, 2-methylimidazole, and ethanol were purchased from Merck, Germany. Sodium dodecyl sulfate (SDS) and propidium iodide were acquired from Sigma-Aldrich.

2.2. Synthesis and Characterization of Ag-MAF Nanoparticles

The metal solution was prepared by dispersion of 0.17 g of $AgNO_3$ in water (30 mL). The ligand solutions were prepared separately by dissolving 0.082 g of 2-methylimidazole in 30 mL of ethanol and 0.118 g of benzimidazole in 40 mL of ethanol, respectively. Ligand and metal solutions were sonicated for 2 min, then mixed at room temperature and stirred for 30 min. The precipitate was then collected, washed with deionized water and ethanol five times, and finally, air-dried. The silver azolate frameworks comprising 2-methylimidazole ligand are labeled MAF-2Imid, while the MAFs consisting of benzimidazole are labeled MAF-Benz. Fig. 1 schematically shows the Ag-MAF synthesis steps.

2.3. Characterization of the Nanoparticles

Attenuated total reflectance-FTIR (ATR-FTIR spectroscopy (Varian Excalibur FTS-3000) was used to study the functional groups of the MAFs structures. To determine the crystalline structure of MAFs, X-ray powder diffraction (XRD) spectra were obtained at 298 Km 40 mA and 40 kV with an XPERT-PRO X-ray diffractometer equipped with a Cu-Kα radiation source (λ = 1.5406 Å). Transmission electron microscopy (TEM) (Zeiss EM900) and field emission scanning electron microscopy (FE-SEM) (MIRA3 TESCAN) equipped with energy-dispersive X-ray spectroscopy (EDX) were applied to analyze the morphology of the MAF samples. The average size distributions of MAF NPs were investigated with dynamic light scattering (DLS) (Nano ZS ZEN 3600). X-ray photoelectron spectroscopy (XPS) (Bestec, Germany) equipped with a 100 μm monochromatic Al-Kα X-ray photoelectron spectrometer source was applied to identify the characteristic elements of the MAF structures.

2.4. Membrane functionalization

Surface modification was carried out by incorporation of MAF-2Imid and MAF-Benz NPs in the surface layer of the membrane. The TFC FO membrane fabrication included two steps. First, a PES ultrafiltration support layer was fabricated by non-solvent-induced phase separation (NIPS). The PES solution (14 wt% PES and 86 wt% DMF) was cast on a clean glass plate with a casting knife (100 μm gate height) followed by immersion in a water coagulation bath at room temperature. Second, the PA active layer was formed by interfacial polymerization (IP) on top of the PES support. To this purpose, the PES support membrane was taped onto a glass plate and then immersed in 30 mL of MPD aqueous solution (2.0 wt%) for 2 min. The excess MPD solution was removed from the PES membrane surface using an air knife. Then, the membrane was immersed in a 0.1 wt% TMC solution (hexane) for 30 s. The membranes were then heat-cured at 80 °C for 5 min. This procedure resulted in a pristine (blank) TFC membrane, used for control experiments.

For the fabrication of the TFN membranes, the same procedure was followed, except 0.03 or 0.06 wt% of MAF-2Imid and MAF-Benz NPs were separately dispersed in the MPD solution. The mixture of MPD and NPs were sonicated for 20 min in an ice-bath before use. The TFN membranes are referred to as Ag-2Imid-3 (0.03% wt% of MAF-2Imid), Ag-2Imid-6 (0.06% wt% of MAF-2Imid), Ag-Benz-3 (0.03% wt% of MAF-Benz), Ag-Benz-6 (0.06% wt% of MAF-Benz).

2.5. Membrane characterization

Thermo Scientific™, Apreo, scanning electron microscope equipped with an EDX detector was applied to characterize the surface and cross-sectional morphologies of the membranes. Atomic force microscopy (AFM, EasyScan II, Swiss) was used to determine their surface roughness. To minimize the experimental error, the surface roughness was determined for three separate membranes. The surface chemistry of the membranes was analyzed by ATR-FTIR (Thermo Scientific USA). The surface charge was assessed with a SurPASS electrokinetic solid surface zeta potential analyzer (Anton Paar USA, Ashland, VA). All the streaming potential measurements were conducted in a background electrolyte solution of 1 mM KCl at 25 °C, over a pH range of 4–9. The

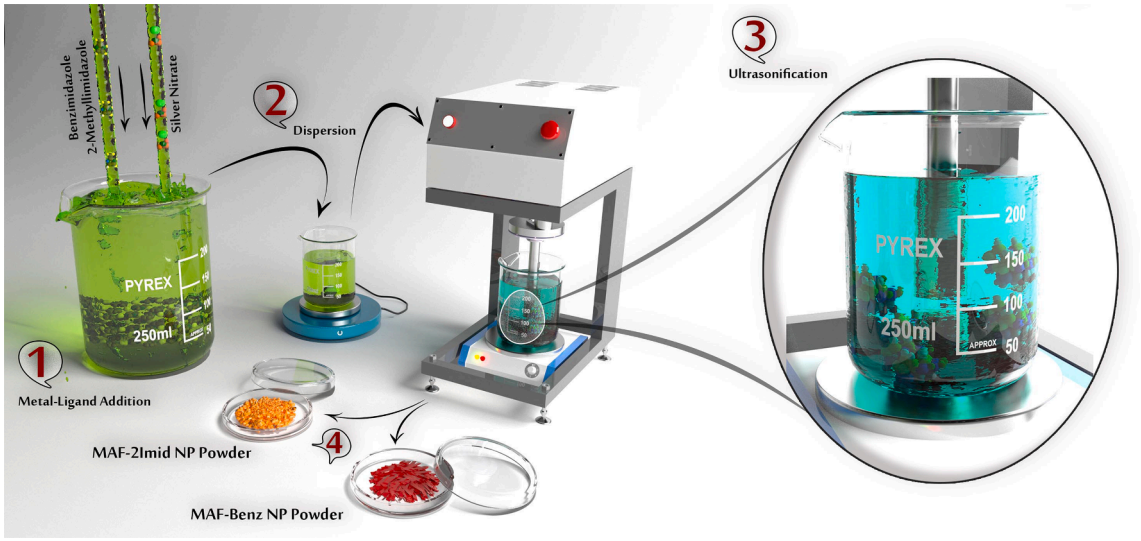

Fig. 1. Schematic illustration of MAF-Benz and MAF-2imid fabrication procedure. Steps 1, 2 involved metal and ligand individual dispersion followed by mixing of the two solutions; these steps were followed by (3) ultrasonication and (4) final powder washing and drying.

zeta potentials of the membranes were calculated based on the Helmholtz-Smoluchowski equation. Two separate samples of each membrane were assessed to account for experimental error. The membrane surface wettability was assessed by means of contact angle measurements (Dataphysics, OCA 15 plus), whereby an average value was calculated from measurements at five random positions. The elemental composition and chemical bonding information of the membrane surface, as well as the release of silver ions from the membrane structure, were evaluated with X-ray photoelectron spectroscopy (XPS, Bestec, Germany).

2.6. Measurements of transport, fouling, and biofouling behavior

The solute permeability (B) and water permeability (A) coefficients, as well as the antifouling and anti-biofouling properties of the membranes, were evaluated with an FO setup following the protocol discussed in our previous study [20,23]. *E. coli* bacteria (10^7 cfu/mL) and sodium alginate (250 mg/L) suspensions were used for accelerated biofouling and fouling experiments, respectively. The fouling experiments were performed for 24 h, the crossflow velocity was set around 8.5 cm/s, and the draw solution concentration was slightly adjusted for different membrane samples to obtain the same initial water flux for the various membranes in fouling and biofouling tests.

2.7. Evaluation of the antimicrobial activity of the membranes

E. coli (ATCC® 10536™) and *P. aeruginosa* (PA14) bacteria strains were used to evaluate the antibacterial properties of the membranes. A colony of *E. coli* was cultivated overnight (16–17 h) in the LB broth Miller medium (Fisher BioReagents™; Cat. No.: BP9723-2) at 37 °C with a stirring rate of 160 rpm. A 1:10 dilution of the culture was prepared in phosphate-buffered saline (PBS) with an approximate density of 10^8 cells/mL. 200 μL of the bacteria sample was added onto a 1 × 1 cm^2 membrane sample and placed in the dark at room temperature for 3 h. To avoid evaporation of the samples, these were placed in a secondary plate covered with a lid. After the 3 h treatment, samples were stained with 5 μM 4′,6-diamidino-2-phenylindole (DAPI, Invitrogen™; Cat. No.: D3571) and 20 μM propidium iodide (PI) (Acros Organics; Cat. No.: 440300250) in PBS for 30 min. Each sample was covered by a microscope glass coverslip and epi-fluorescence images were collected by a 40× lens (Plan Fluor, 40x/0.75) under an EVOS scope. DAPI and Texas Red channels (70% light intensity; 500 ms exposure time) were used to record the number of live (DAPI-stained) and dead (PI-stained) cells in each FOV. The average percentage of dead cells was determined for at least ten FOVs for each sample.

To assess the biofilm inhibition properties of the membranes, a colony of PA14 was cultivated overnight (16–17 h) in the LB broth Miller medium (Fisher; Cat. No.: BP9723-2) at 37 °C with a stirring rate of 160 rpm. A 1:100 dilution of the culture was prepared in M9 minimal medium with an approximate density of 10^7 cells/mL. Five mL of the bacteria sample was added onto a 1 × 1 cm^2 membrane samples in a 6-well plate and placed in the dark at room temperature for 48 h. The planktonic bacteria were washed with sufficient PBS and biofilms were then stained with 5 μM DAPI for 30 min in the dark. The excess DAPI was washed with sufficient PBS and epi-fluorescence images were collected with a 10 × lens to visualize bacteria biofilms. At least ten field of views were examined for each sample.

2.8. Chemical stability of the TFN membranes

The chemical stability of the TFN membranes was preliminarily investigated by determining the amount of silver ions released from the TFN membranes. A sample of each membrane (circular sample with a diameter of 2 cm) was stored in 20 mL of DI water with continuous shaking (150 rpm) for 30 days. The concentration of silver ions in the DI water solution was determined by inductively coupled plasma mass spectrometry (ICP-MS, AA300 Agilent Technologies).

3. Results & discussion

3.1. Membranes physiochemical characterization

The FTIR spectra (Fig. 2) of the pristine (blank) membranes and of the membranes prepared with two different concentrations of the MAF-2Imid and MAF-Benz NPs showed a broad peak around 3300 cm^{-1}, representing O—H stretching [24]. The peaks between 1150 and 1320 cm^{-1} detected in all membranes are mostly associated with the PES support: for example, the peak at 1319 cm^{-1} corresponds to O═S═O asymmetric stretching vibration [20,25–26]. The observed peak at 1237 cm^{-1} is assigned to C—O—C symmetric stretching [26]. The band at 1483 cm^{-1} is most likely attributed to C═O stretching vibration present in the amide [24]. The peak associated with N—H stretching was detected at 1610 cm^{-1} [27]. The peak at 1575 cm^{-1} is ascribed to N—H bending [27–28] and also C═N stretching present in imidazole structure

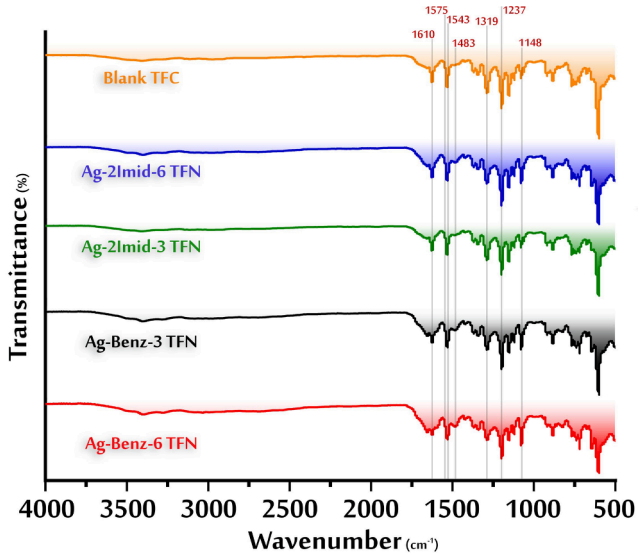

Fig. 2. FTIR spectra of membranes.

[29], which is the reason why this peak was more intense for modified membranes. The bands at around 1000 and 1148 cm^{-1} are attributed to the C—N bending and C—N stretching, respectively [30–31]. The peak at 1148 cm^{-1} can also be overlapped by the peak of O═S═O symmetric stretching vibration in the PES [26]. Furthermore, the appearance of a peak with a subtle intensity at around 1543 cm^{-1} is most likely due to possible interactions between NPs and the polyamide network as this peak was not observed in the blank TFC membrane spectrum [20].

XPS measurements were performed in order to analyze the elemental composition and chemical bonds of the membranes (Fig. 3). High-resolution spectra of modified membranes showed signals at binding energies of 366 eV (Ag $3d_{5/2}$) and 372 eV (Ag $3d_{3/2}$), which corroborate the presence of silver on the modified membranes [20]. The other XPS dominant peaks are related to carbon, nitrogen, and oxygen (peaks approximately at 283, 398, 530 eV for C 1 s, N 1 s, and O 1 s, respectively), which are observed in all the spectra since these elements are the PA layer constituents.

High-resolution C 1 s, N 1 s, and O 1 s XPS spectra are shown in Fig. 3**b-d**. The profiles related to C 1 s indicate two signals in which the major peak centered at 283 is assigned to C—H, C—C, C═C [32–33], and C—N bonds [34]. The minor peak, approximately at 286 eV, is attributed to C—O, C—O—C, O—C═O, C—O—H, C═O, and C═N bonds [20,33]. Fig. 3**b** shows the deconvoluted XPS spectra of the O 1 s range in which the first peak around 530 eV is attributed to N—C═O, O—C═O, and C═O bonds, and the second peak around 531.5 eV is correlated to O—C═O and C—O—H bonds [35]. In addition, high-resolution XPS spectra of the N 1 s region indicate the peak at 398 eV, which is mostly attributed to N—H and N—C bonds [32,34]. The N 1 s signal of the membrane modified by more concentration of benzimidazole consists of two peaks located approximately at 398 and 400 eV (Fig. 3**d**). The first peak is additionally assigned to the N atoms in the

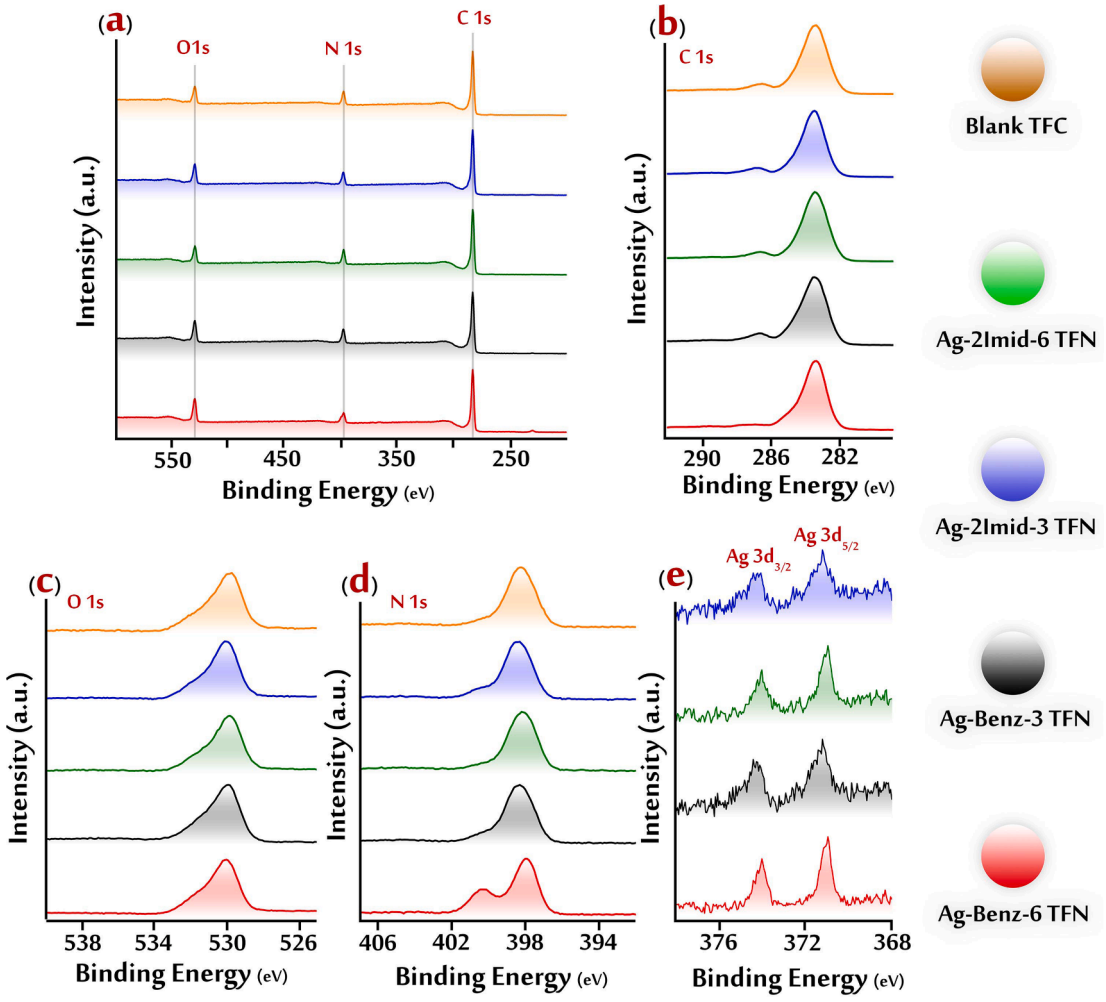

Fig. 3. a) XPS survey spectra of the membranes. Deconvoluted high-resolution XPS spectra of b) C 1s, c) O 1s, d) N 1s, and e) Ag 3d.

imidazole ring [36–37]. The second peak appearing for the functionalized membrane and with the higher binding energy is mainly assigned to the nitrogen in the imidazole ring coordinated with silver (N–Ag) [38], which results in the peak shift to higher binding energy. Noticeably, this peak was barely visible in the XPS spectrum of the membrane modified by a lower concentration of benzimidazole; on the other hand, XPS silver atom signals were more intense for the membrane modified by a higher concentration of benzimidazole.

Table 1 summarizes the elemental compositions of the membranes. The O/N ratio of PA theoretically varies between 1 (fully crosslinked) to 2 (fully linear) [39]. The degree of crosslinking reflects the density of the PA structure and may be correlated to the membrane selectivity (higher degree of crosslinking should reflect in higher selectivity), whereas a lower crosslinking may be related to higher hydrophilicity and water flux. Table 1 also indicates the ratio of silver atoms peak intensities, from XPS spectra shown in Fig. 3**e**, indicating that both Ag-Benz-3 and Ag-Benz-6 TFN membranes had higher concentrations of silver in their outermost layer than Ag-2Imid-3 and Ag-2Imid-6 TFN membranes, despite the fact that for each separate pair of TFN membranes the same amount of Ag-MAFs was added during fabrication. Fig. 4 also shows the relevant EDX spectra and EDX mapping of TFN membranes, clearly supporting the presence of silver and other relevant atoms at the membrane surface.

SEM cross-sectional and surface micrographs of the TFN membranes are reported in Fig. 5. The blank TFC membrane and all TFN membranes exhibited a typical ridge-and-valley morphology, which is the common structure of PA membranes [39]. Brighter spots can be observed on the surface of TFN membranes upon the incorporation of NPs in the PA layer, which can be attributed to the presence of silver. Such brighter features are more easily detected in the cross-sectional SEM images, especially for the Ag-2Imid-3 TFN membrane. These results may indicate the homogenous and high-density dispersion of the MAF-2Imid and MAF-Benz NPs within the PA layer of modified membranes, supporting the hypothesis of efficient compatibility between NPs and PA matrix [40]. The incorporation of the NPs may decrease the MPD diffusion rate and reduce the polymerization rate of the PA layer as a result of steric hindrance of MAF-2Imid and MAF-Benz NPs [41]. These alterations would, in turn, result in higher water flux [42].

From AFM (Fig. 5), the average root means square roughness (R_{RMS}) parameter of the membranes was 58, 66, 71, 89, and 103 nm for blank TFC, Ag-2Imid-3, Ag-Benz-3, Ag-2Imid-6, and Ag-Benz-6, respectively. Obviously, the R_{RMS} increased after the addition of NPs, which is consistent with the SEM images of each membrane. This result is especially dominant for Ag-2Imid-6 and Ag-Benz-6 membranes, which have higher contents of NPs and showed larger R_{RMS} values. This observation may support the idea that the higher concentration of NPs ends in agglomerates formation, especially for Ag-Benz TFN membranes [43]. Also, the higher ratio of silver atoms (from XPS spectra) suggests that more NPs exist on the outmost surface of the Ag-Benz TFN membranes, compared with the Ag-2Imid TFN membranes, which may also be a result of non-uniform NPs distribution in the cross-section of the PA layer. This inhomogeneity can affect the performance of the membrane in terms of permeability and selectivity [44]. Also, membranes with rougher surfaces have been reported to be generally more inclined to biofouling by macromolecules and bacterial cells [23]. However, there is no straightforward relationship between fouling behavior, roughness, or hydrophilicity [11].

Table 1
O/N ratio, elemental compositions, and Silver atom intensity ratio of the TFC and TFN membranes.

Membrane	Atomic concentration (%)				O/N ratio	Ag ratio (from spectra intensity)
	C (1 s)	O (1 s)	N (1 s)	Ag (3d)		
Blank TFC	63.4	21.0	15.6	–	1.3	–
Ag-2Imid-3TFN	61.9	23.0	14.4	0.7	1.6	Ag-2Imid-6/Ag-2Imid-3: **1.2**
Ag-2Imid-6-TFN	63.2	20.7	15.2	0.9	1.3	Ag-Benz-3/Ag-2Imid-3:**1.5**
Ag-Benz-3 TFN	58.8	24.8	15.4	1.0	1.6	Ag-Benz-6/Ag-Benz-3: **1.4**
Ag-Benz-6-TFN	61.8	24.8	12.0	1.4	2.0	Ag-Benz-6/Ag-2Imid-6:**1.8**

To assess the surface wettability of the membranes, the water contact angle of the membranes was measured, and results are shown in Fig. 5**p**. The average contact angle reduced from 74.1° for the blank TFC membrane to 60.1°, 50.4°, 33.2°, and 28.6° for Ag-2Imid-3, Ag-2Imid-6, Ag-Benz-3, and Ag-Benz-6 TFN membranes, respectively. This improvement in the membrane wettability is attributed to the incorporation of the hydrophilic NPs. Both MAF-2Imid and MAF-Benz NPs contain hydrophilic functional groups on their structure that increase the chance for hydrogen bonds interactions with water molecules [23]. Although all the TFN membranes showed a rougher surface than the blank TFC membrane, wettability may overwhelm the effect of surface roughness in case of biofouling mitigation [11].

Surface charge is another important property of membranes, affecting the rejection of charged contaminants and foulants [45]. Bacterial cells usually carry a negative surface charge in a pH range of 4–9: addition of negatively charged additives can improve the antibiofouling properties of the membranes by exploiting the electrostatic repulsion [46]. Fig. 5**q** presents the value of zeta potential for the membranes in the pH range 3–11. The carboxyl groups of the PA layer deprotonate at increasing pH [47]. What stands out in Fig. 5**q** is the more negative zeta potential of all the TFN membranes compared to the blank TFC membrane. This result can be attributed to the contribution of functional groups of MAF-2Imid and MAF-Benz present in the structure of NPs. The Ag-Benz-6 TFN membrane was characterized by the largest negative surface charge, which can be attributed to the higher density of MAF-Benz-6 NPs within the active layer and their closer distance from the surface [48]. This improvement in surface charge of all TFN membranes can eventually result in stronger antibiofouling properties.

3.2. Biofilm Inhibition and Antibacterial Properties of MAF-enabled Membranes

The effective MAF incorporation into the polyamide active layer is hypothesized to impart antibacterial properties to the membrane, suitable for biofilm inhibition, and the results of this assessment are summarized in Fig. 6. An anti-biofouling membrane should be able to both inactivate bacterial cells that come into contact with its surface and inhibit the growth and multiplication of any cells that manage to deposit.

To first examine the antibacterial properties of the TFN membranes against planktonic cells, we used *Escherichia coli* (*E. coli)*, a common strain with medium to low tendency to make biofilms on surfaces. The viability of bacterial cells upon contact with the membranes was tested by imaging the cells after staining with propidium iodide (PI) and 4′,6-diamidino-2-phenylindole (DAPI) molecules. Both fluorophores exhibit fluorescence enhancement upon intercalation into double-stranded regions of DNA (DAPI-stained is blue; PI-stained is red) [49]. Considering that the cytoplasmic membrane of bacterial cells is permeable to DAPI but not PI, PI fluorescence enhancement is observed only if the integrity of the cytoplasmic membrane is lost, an indication of the inactivation of bacteria.

E. coli bacteria, suspended in an aqueous medium, were exposed to the membrane surface for 3 h in the dark to minimize the effect of oxidative stress (e.g., provided by reactive oxygen species) [50–51]. While the majority of bacteria (>97%) in contact with the blank TFC membrane were stained only by DAPI molecules (Fig. 6**b**), a significant portion of the cells in contact with TFN membranes were stained by PI, indicating their inactivation (Fig. 6**c-f**). Fig. 6**g** summarizes the percentage of viable *E. coli* cells calculated from these data. Specifically,

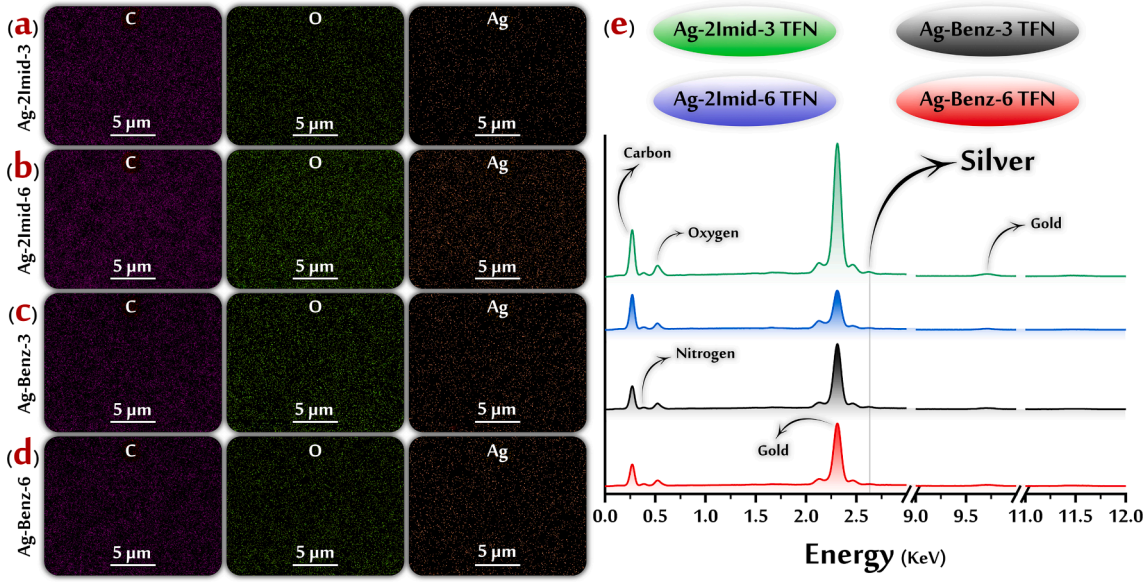

Fig. 4. a-d) Carbon, Oxygen and Silver EDX mapping of TFN membranes, e) EDX spectra of TFN membranes.

60%, 47%, 22%, and 18% of the cell population was viable after exposure to Ag-Benz-3, Ag-Benz-6, Ag-2Imid-3, and Ag-2Imid-6 TFN membranes, respectively. Overall, Ag-2Imid membranes showed higher damaging potential toward planktonic *E. coli* compared to Ag-Benz.

Furthermore, we examined the ability of the membranes to inhibit the formation of a biofilm by *P. aeruginosa,* a ubiquitous Gram-negative bacterium known for forming robust biofilms [13,52]. As a human opportunistic pathogenic bacterium, *P. aeruginosa* is responsible for both acute and chronic infections, including serious complications in burns, eye lesions, and cystic fibrosis lungs [2,24–25]. Beside its natural resistance to several drugs [28], it is capable of producing strong biofilm structures that facilitate infection and aid the microorganism in withstanding antimicrobial treatment and host defences [30]. Fig. 6**h** displays a blank TFC membrane that was fully covered by a *P. aeruginosa* biofilm within 48 h. In this experiment, DAPI stained both bacterial cells and extracellular polymeric substances (EPS) within the biofilm structures. Cells and EPS are indicated by a yellow and red arrow, respectively, in Fig. 6**i**. TFN membranes, in contrast, provided strong inhibition against biofilm formation. While small pieces of thin biofilms (10–50 µm wide) were observed on Benz- TFN membranes (Fig. 6**j, and k**), negligible biofilm was present on the 2Imid- TFN membranes (Fig. 6**l, and m**). Biofilms were semi-quantitatively determined by measuring the fractional blue area in each field-of-view (FOV): on the basis of this assessment, Ag-Benz-3, Ag-Benz-6, Ag-2Imid-3, and Ag-2Imid-6 TFN membranes resulted in ~ 90%, 95%, 99%, and 99% inhibition of biofilm formation. Overall, these results corroborated the initial hypothesis: successful incorporation of antimicrobial MAFs provided the membranes with promising antibacterial properties. Similar to *E. coli* results, this effect was more pronounced when deploying MAFs based on the 2-Imidazole ligand.

Fouling and Biofouling Effect on Flux Decline. The static tests discussed above suggest that the membrane surface would act to reduce bacterial growth during operation. However, biofilm formation requires the deposition of cells onto the membrane; a mechanism governed mostly by fluid dynamics and interaction forces (e.g., electrostatic and hydrophobic interactions). Also, bacteria often exploit the pre-deposition of organic foulants to find a hospitable environment at the membrane surface. To gain information on the overall effect of fouling and biofouling on water flux decline, we performed filtration experiments in forward osmosis (FO) configuration and in the presence of alginate or E. coli in the feed solution (Fig. 7a and b, respectively). It is worth noting that our preliminary tests suggested a negligible effect of reverse solute passage and draw solution dilution on flux decline. Hence, the observed flux decline in Fig. 7a,b, might be ascribed solely to fouling-related effects.

As hypothesized, all the TFN membranes showed reduced flux decline compared to the blank TFC membrane. This improvement can be attributed to the combined effects of enhanced wettability of the TFN surfaces (Fig. 5**p**) and reduced bacterial growth (Fig. 6). However, the substantial effect observed in biofouling tests suggests the important role of silver ions in reducing the attachment of the bacterial cells onto the membrane surface and their subsequent growth. TFN membranes improved water flux in tests with sodium alginate and *E. coli* up to approximately 45% and 80%, respectively, with respect to TFC membranes, showing less than 10% overall flux decline (especially for bacterial fouling) after 24 h of filtration under accelerated fouling conditions.

3.3. Membrane transport properties

The main problem encountered during the fabrication of TFN membranes is the aggregation of nanomaterials that typically cause defects in the synthesized polyamide layer [53–54]. The presence of organic ligands in MAFs can improve their compatibility with the polyamide matrix when compared to other inorganic nanomaterials [55]. One of the main hypotheses of this study is that appropriate MAF chemistry will indeed minimize the deterioration of transport properties or even have a positive impact on flux and rejection performance.

The water transport performance of the membranes was studied in a four-step FO protocol [56], and the intrinsic membrane parameters were calculated from water and solute fluxes; see Fig. 7**c-e**. The water permeability coefficient, A, increased from 0.3 for blank TFC to 0.7 and 1.3 L $m^{-2}h^{-1}bar^{-1}$ for Ag-2Imid-3 and Ag-Benz-3 TFN membranes, respectively, while the solute permeability coefficient (B) slightly increased from 0.2 to ~ 0.5 L $m^{-2}h^{-1}$. The water and solute fluxes of the Ag-Benz-6 TFN membrane had large variability and could not be adequately modeled. As a result, the B/A ratio, a parameter that simply indicate the membrane selectivity and that should be as low as possible, decreased for both Ag-2Imid-3 and Ag-Benz-3 TFN samples, compared to blank TFC, but it increased for Ag-2Imid-6 TFN, suggesting poor selectivity for the latter membrane. Please note that improvement in selectivity was obtained in combination with an increase in permeance for some membranes, which would result in higher membrane productivity at equivalent or better permeate quality. These results

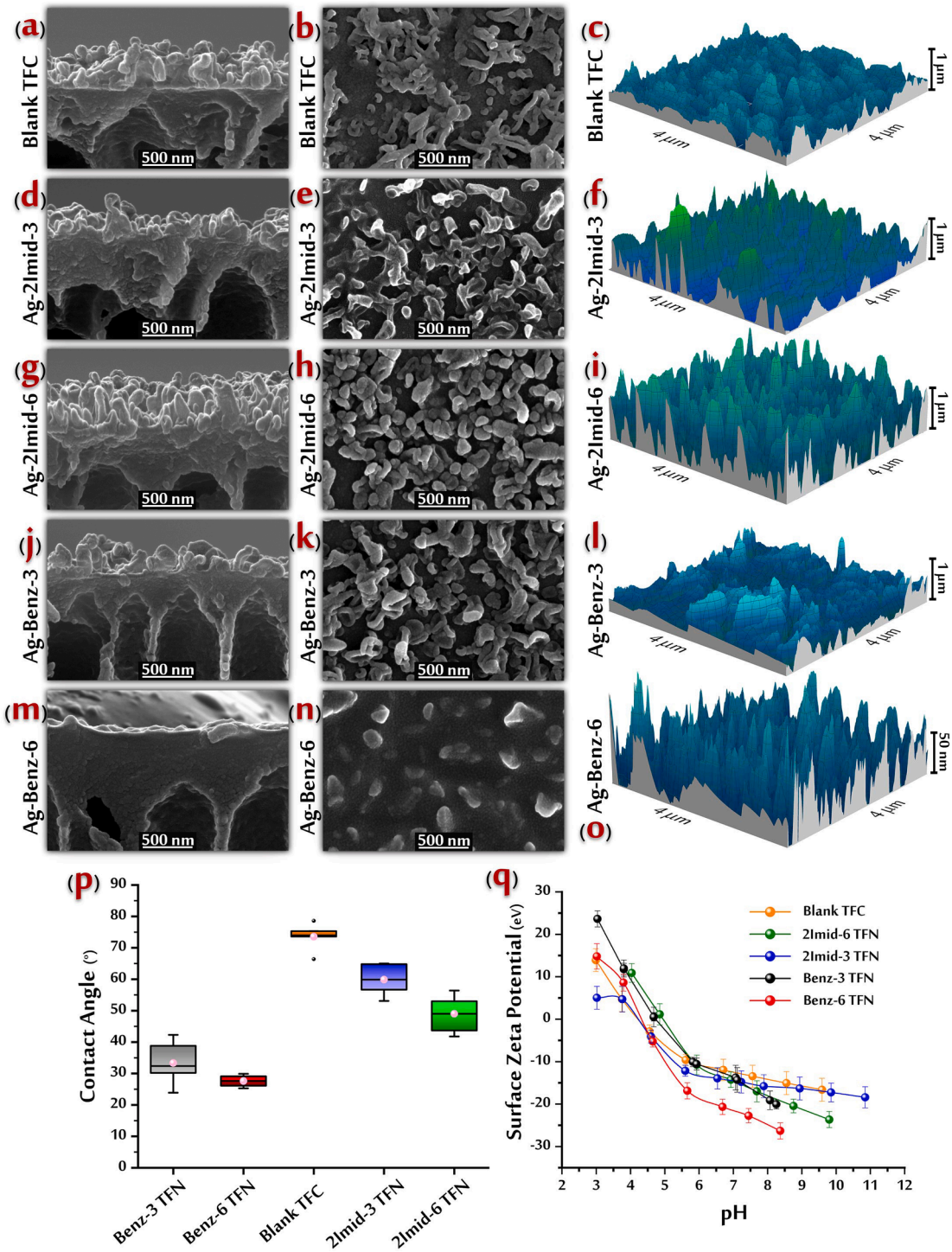

Fig. 5. a-o) Cross-sectional SEM, top surface SEM, and AFM images of membranes; p) contact angle measurements of water sitting on the surface of the various membranes; q) zeta potential measurements of the membranes surface.

demonstrate improvement in the performance of the TFN membrane, but only in the case of the lesser (0.03%) of the MAF concentrations incorporated during the interfacial polymerization (IP) reaction.

The results reported here demonstrate that functionalization of TFN membranes with MAF-2Imid and MAF-Benz can inhibit the growth of both planktonic bacteria and the robust biofilm-forming bacterium *P. aeruginosa,* and mitigate flux decline due to organic fouling and biofouling. Structure and antimicrobial activity of these MAF NPs are summarized in Fig. 8**a-d** and supporting information. MAF-2Imid showed an octahedral structure with an average particle size of around 760 nm and thickness of MAF-Benz nanoribbons in the range 160–190 nm, with an average particle size of 550 nm. TEM and FE-SEM results of these nanoparticles are consistent with the assumptions regarding their 3D structure. As with other types of nano-additives, surface modification with MAFs alters the polyamide layer structure based on one or more of the following three mechanisms; I) changing the kinetics of IP reaction, II) interaction of nanofillers with the PA matrix and affecting the network and aggregate pores, and III) alterations in the hydrolysis degree of acid chloride [57]. Concerning the first mechanism, the presence of nanoparticles during IP may change the penetration rate

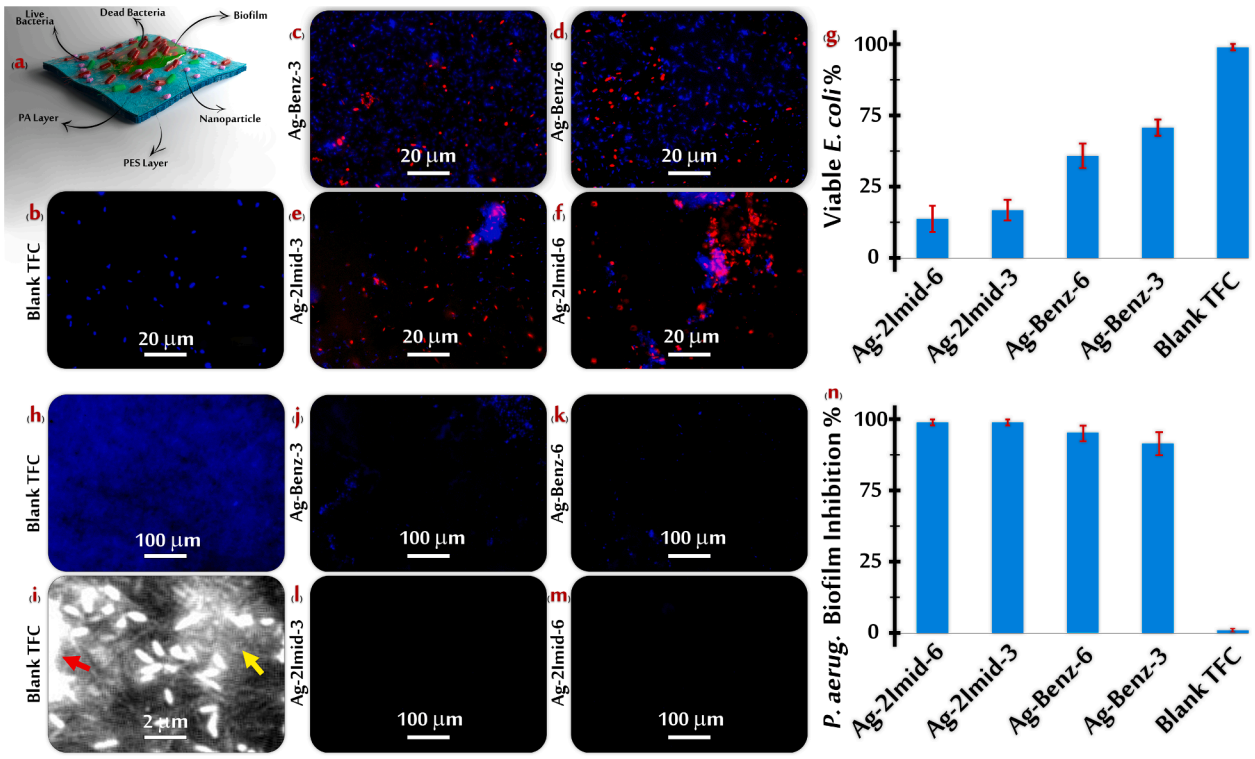

Fig. 6. (a) Illustration of biofilm formation and mitigation on membranes; (b-f) fluorescence imaging results obtained upon exposure of *E. coli* planktonic cells to the antibacterial membranes. The dead bacteria cells are colored in red while the live bacteria are in blue. (g) Percentage of viable *E. coli* cells; (h-m) *P. aeruginosa* biofilm formed on the membranes. Blue spots represent the biofilm. (n) Resulting percentage of biofilm inhibition by the membranes. (For interpretation of the references to colour in this figure legend, the reader is referred to the web version of this article.)

of TMC/MPD monomers into the reaction zone, and a looser layer may form [58]. This mechanism may be controlled by suitable dispersion of the nanoparticles in the monomer solutions and by adopting appropriate concentrations. The second and third mechanisms may be controlled by careful choice of the organic linker of the nanostructures. Good compatibility with the surrounding polyamide will allow the formation of a seamless selective layer, enabling the MAFs to be incorporated without adverse effects on permeation properties. The rationale is that the organic linker should be chosen to interact with the polyamide chains during membrane formation and in the final layer, thus minimizing defects and discontinuities in the membrane active film. In this study, the methyl and amine functional groups on the surface of MAF-2Imid and MAF-Benz NPs, respectively, most likely interacted with amine and carbonyl/carboxyl groups of the PA layer, along with possible π- π interaction of PA benzene rings with MAF-Benz NPs [59–60]. These chemical interactions would be expected to improve the compatibility and dispersion of MAF-2Imid and MAF-Benz in the PA matrix. Fig. 8**e1, and 8e2** illustrates possible chemical interactions between these two NPs and the PA chains.

The better biofouling inhibition and bacterial inactivation observed with Ag-2Imid membranes are consistent with our observations of NP antibacterial performance shown in Fig. 8**c and d**, implying that MAF-2Imid nanoparticles have higher intrinsic antibacterial activity compared too MAF-Benz particles. This result can be explained by the intrinsic antimicrobial properties of the imidazole ligand [22]. This molecule can enter living bacterial cells by passive diffusion and produce nitro radical anions, which can, in turn, oxidize the DNA or rupture the cell wall to cause the damage and death of the cell [22]. Another hypothesis suggests that the imidazole rings interact with the flavohaemoglobins present in the bacterial cells and inhibit the nitric oxide dioxygenase function, thus preventing the metabolism of nitric acid leading to the death of the cells [22]. That being said, in the case of MAF-Benz and MAF-2Imid nanoparticles containing silver, the dominant role in antimicrobial activity may be attributed to silver, and possibly to the coordination ability of silver ions to O, N, or S donor atoms, as well as hydroxyl, carboxyl, sulfhydryl, and amino functional groups available in the bacterial cell membrane or DNA, leading to inhibition of bacterial functions [22].

A promising feature of TFN membranes is their potential to prevent biofilm growth during long-term operation. MAF-2Imid and MAF-Benz particles may act as reservoirs of silver, promoting the sustained and gradual leaching of this metal ion to achieve prolonged antibacterial activity of the membrane (Fig. 9). The bacterial inactivation rate may be correlated with the release rate of silver ions. However, a suitable balance should be found between silver-mediated antibacterial activity (i.e., leaching rate) and long-term functionality. To provide insight into this feature, silver leaching tests were carried out for a period of 30 days with both Ag-2Imid-3 and Ag-Benz-3 TFN membranes. Both membranes presented the same trend of the initial decrease in ion release rate for the first 7 days (Fig. 9**)**. The samples showed a similar behavior characterized by an overall low leaching rate, with this mechanism being slightly faster for the Ag-2Imid-3 TFN membrane. The slow release observed for the membranes allows prolonged antibacterial properties during operation, while providing sufficient activity to inhibit bacterial proliferation, as suggested by the results presented in Fig. 6. It is important to clarify that membrane antibacterial activity may not directly translate into lower flux decline during filtration. Bacterial growth is only one of the steps involved in biofilm formation, the first being attachment of bacteria and other foulants onto the membrane surface. Therefore, preventing this initial seeding phenomenon is also essential. While analogous flux decline was observed with Ag-2Imid-3 and Ag-Benz-3 TFN membranes in the presence of biofoulants, the latter showed reduced flux decline in the presence of alginate, probably due to the improved wettability of its surface, another critical issue provided by the presence of the MAF structures deployed in this study.

In terms of membrane transport performance, an advantageously

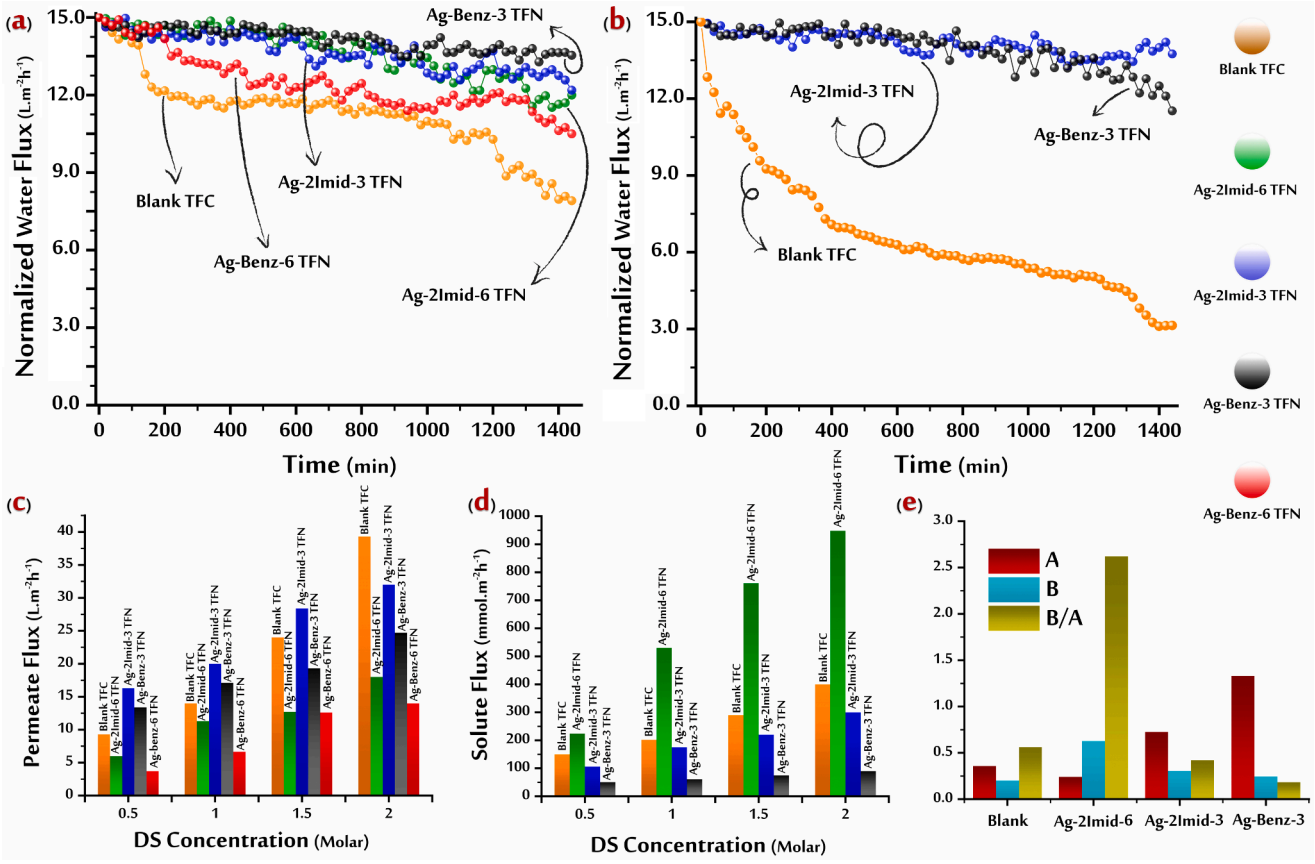

Fig. 7. Membrane transport properties in forward osmosis tests using 1 M NaCl as a draw solution. Flux decline due to (a) organic fouling by alginate, (b) bacterial fouling by *E. coli*. The results are the average of 3 separate experiments. (c) Experimental steady-state water flux measured with water as feed solution and a different draw solution concentration for each measurement step; (d) experimental steady-state reverse solute flux; resulting (e) transport parameters of the membranes: A (water permeability coefficient (L $m^{-2}h^{-1}bar^{-1}$)); B (solute permeability coefficient (L $m^{-2}h^{-1}$)). The results are the average of 3 separate experiments.

lower B/A ratio was observed for Ag-2Imid-3 and Ag-Benz-3 TFN membranes, together with larger water fluxes compared to the blank TFC membrane (Fig. 7) [61]. This improvement in transport properties may be attributed to the I) improvement in the hydrophilicity of TFN membranes, II) formation of nano-sized voids at the interface of NPs and PA matrix, and III) favorable modification of the morphology and structure (e.g., thickness, density, homogeneity) of the overall active layer in the presence of MAF NPs during membrane synthesis. The formation of large NP aggregates and their inhomogeneous distribution into the PA layer would lead to weak compatibility and reduction in the membrane performance [62]. While increasing the concentration of NPs in the membrane could possibly increase the bactericidal potential (Fig. 6), increasing MAF concentration has potential disadvantages for PA layer formation, transport properties and costs. Lower MAF concentrations are likely to reduce NP agglomeration, enabling more even distribution of MAFs, more consistent PA layer formation, and possibly superior transport properties.

Fig. 10**a, and c** schematically represents the possible 3D structure of TFN membranes along with the possible key factors affecting their long term performance (Fig. 10**b**). The four parameters are well-documented to affect membane fouling. Higher wettability and electrostatic repulsion minimize the rate of bacterial attachment; increased inhibition of planktonic bacteria decreases the adhesion rate of bacteria on the membrane surface of membrane, further decreasing the chance of fouling. Unlike these three factors, a change in surface roughness can have either positive and negative effects on transport; rougher surfaces may provide more surface available for water passage but it is important to note that the rougher surfaces characterizing TFN membranes may partly thwart the positive effects of surface wettability and promote some deposition of foulants onto the surface depressions of the resulting layer. Similar to MPD monomers, both MAF-2Imid and MAF-Benz nanoparticles carry amine functional groups. These groups are likely react with the TMC monomers during layer formation, and some additional hydrogen and covalent bonds form between NPs and PA chains. Their compatibility is indirectly demonstrated by the low salt flux, indicating no or negligible defects in the layer. The durability of the TFN membrane was instead investigated by monitoring the silver ion release for 30 days to support this hypothesis. The results of the experiments suggest the suitable integrity and prolonged antimicrobial activity of the TFN membranes.

4. Conclusion

Here we provide the first demonstration of a functionalized PA membrane that simultaneously can maintain high selectivity, achieve almost complete suppression of the growth of a robust biofilm forming bacterium, inactivation of planktonic bacteria, and retain flux under the simulation of long-term organic fouling and biofouling. The best improvements were actually achieved with low concentrations of modifying agents, specifically, only 0.03% mass of additives, and little generation of hazardous waste products, demonstrating that low-cost and environmentally benign functionalization can greatly enhance PA membrane performance. The membranes with 0.03% MAFs (Ag-2Imid-3 and Ag-Benz-3) yielded the best performance. Therefore, further research is needed to determine the ideal concentrations to optimize performance for various applications, feed solutions and performance goals.

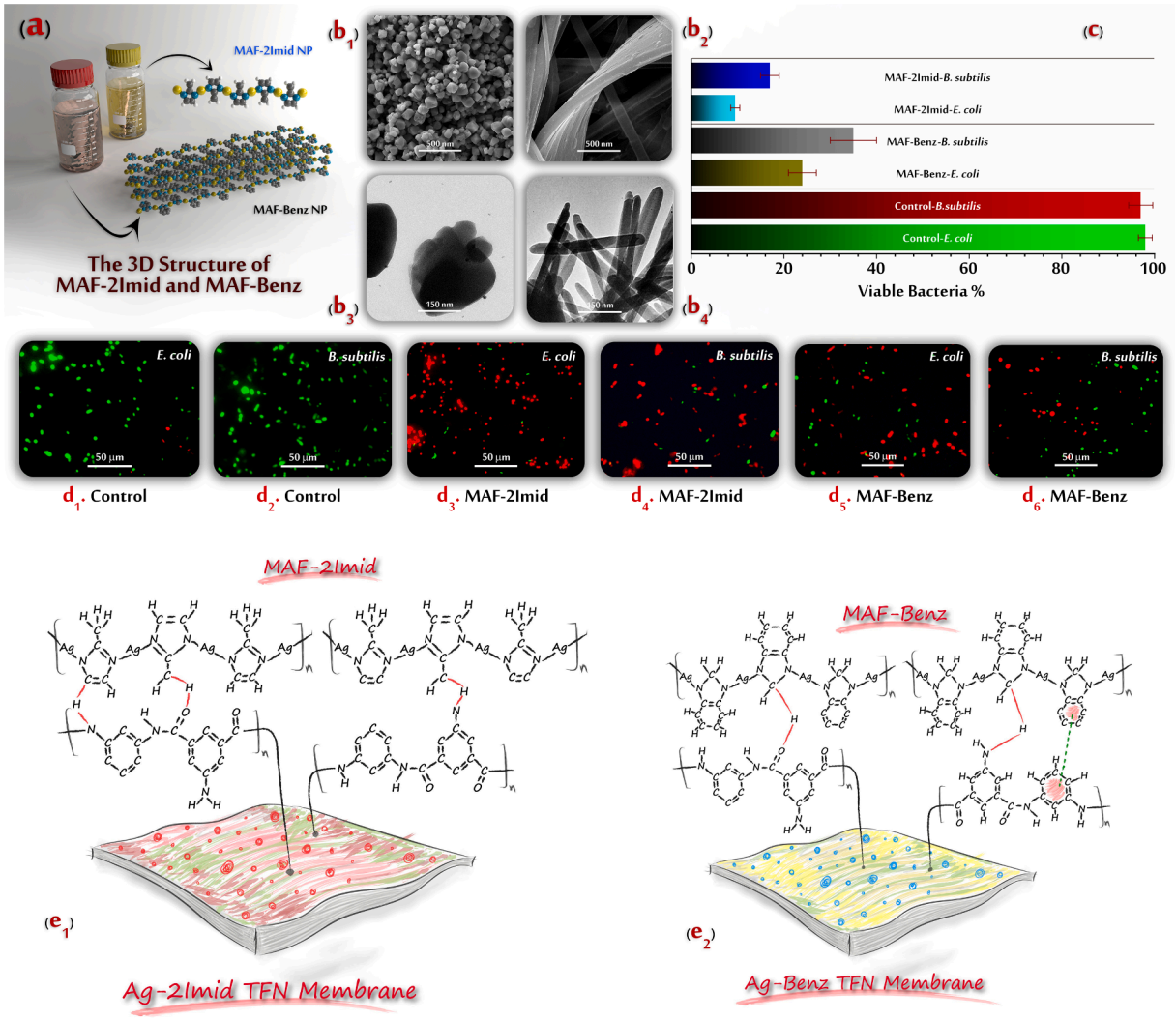

Fig. 8. (a) Schematic illustration of 3D structures and characteristics of MAF-Benz and MAF-2Imid nanoparticles: b_1) SEM images of MAF-2Imid, b_2) SEM images of MAF-Benz, b_3) TEM image of MAF-2Imid, b_4) TEM image of MAF-Benz, c) antibacterial activity of MAF-Benz and MAF-2Imid particles against *E. coli* and *B. subtilis* and d_1-d_7) related fluorescence imaging. The dead bacteria cells are colored in red and live bacteria in green. Reproduced with permission from ACS [22]. (e_1-e_2) Schematic illustration of membranes surface chemistry and possible interactions of the metal azolate frameworks with polyamide. (For interpretation of the references to colour in this figure legend, the reader is referred to the web version of this article.)

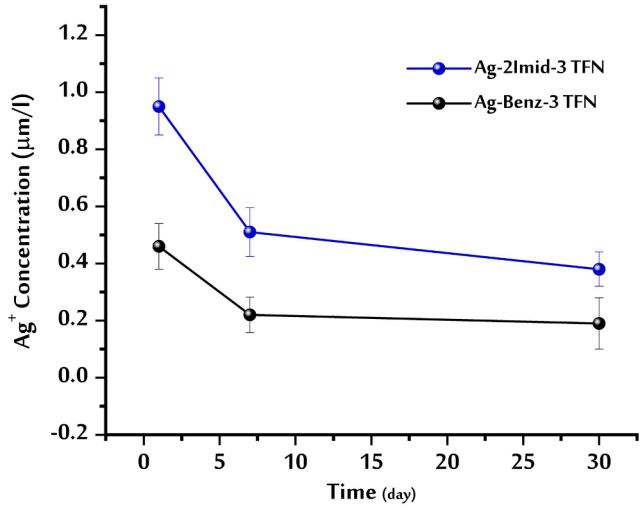

Fig. 9. The release rate of Silver ion measured by ICP-MS for a period of 30 days.

CRediT authorship contribution statement

Mostafa Dadashi Firouzjaei: Data curation, Formal analysis, Investigation, Visualization, Writing – original draft. **Mehdi Pejman:** Data curation, Formal analysis, Investigation, Visualization, Writing – original draft. **Mohammad Sharifian Gh:** Investigation, Data curation. **Sadegh Aghapour Aktij:** Investigation, Visualization, Data curation, Formal analysis. **Ehsan Zolghadr:** Investigation, Validation, Formal analysis. **Ahmad Rahimpour:** Conceptualization, Funding acquisition, Project administration, Resources, Supervision, Visualization, Writing – review & editing. **Mohtada Sadrzadeh:** Validation, Resources, Supervision, Writing – review & editing. **Ahmad Arabi Shamsabadi:** Formal analysis, Supervision, Writing – review & editing. **Alberto Tiraferri:** Conceptualization, Funding acquisition, Project administration, Resources, Supervision, Visualization, Writing – review & editing. **Mark Elliott:** Conceptualization, Funding acquisition, Project administration, Resources, Supervision, Visualization, Writing – review & editing.

Declaration of Competing Interest

The authors declare that they have no known competing financial

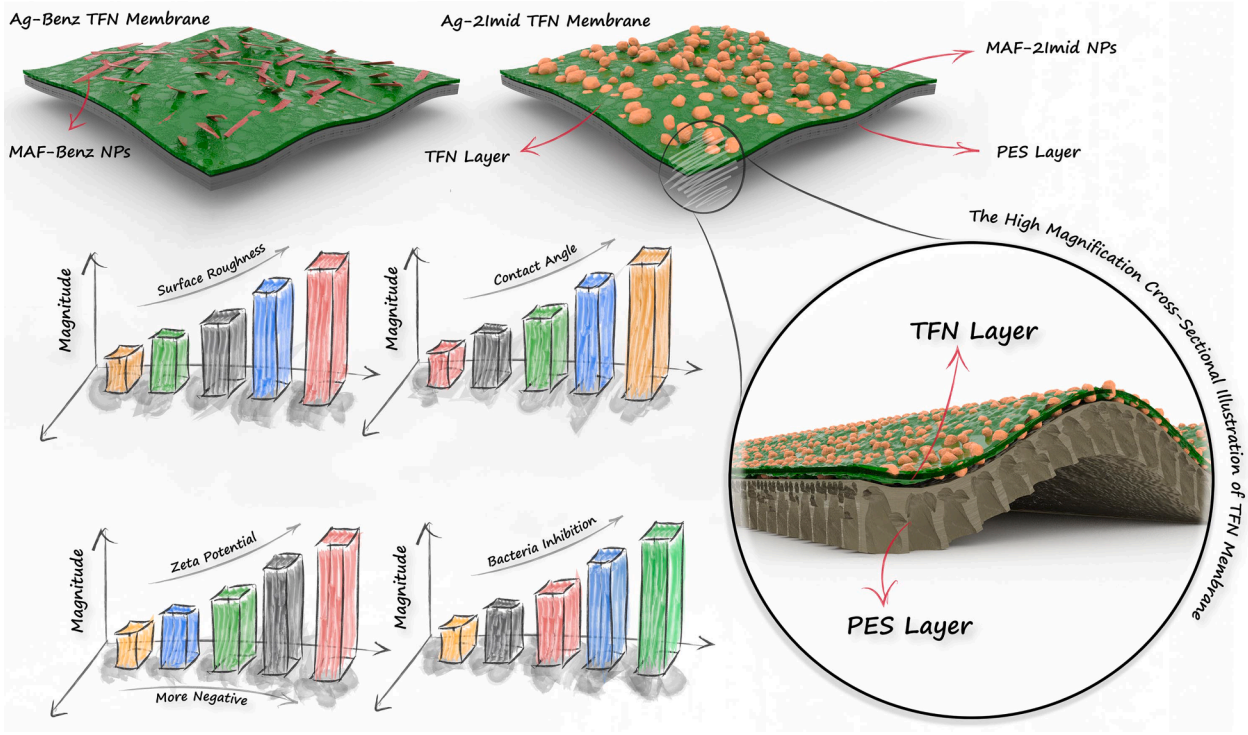

Fig. 10. (a) Schematic illustration of TFN membranes and (b) contributing parameters to antifouling and anti-biofouling performance; (c) high magnification cross-sectional illustration of TFN membranes. Blue: Ag-2Imid-3, Green:Ag-2Imid-6, Black: Ag-Benz-3, Red: Ag-Benz-6, and Orange: Blank TFC. (For interpretation of the references to colour in this figure legend, the reader is referred to the web version of this article.)

interests or personal relationships that could have appeared to influence the work reported in this paper.

Appendix A. Supplementary material

Supplementary data to this article can be found online at https://doi.org/10.1016/j.seppur.2021.119981.

References

[1] J.W. Costerton, Z. Lewandowski, D.E. Caldwell, D.R. Korber, H.M. Lappin-Scott, Microbial biofilms, Annu. Rev. Microbiol. 49 (1) (1995) 711–745.
[2] L. Hall-Stoodley, J.W. Costerton, P. Stoodley, Bacterial biofilms: from the natural environment to infectious diseases, Nat. Rev. Microbiol. 2 (2004) 95–108.
[3] J.J. Harrison, H. Ceri, R.J. Turner, Multimetal resistance and tolerance in microbial biofilms, Nat. Rev. Microbiol. 5 (12) (2007) 928–938.
[4] T.-F. Mah, B. Pitts, B. Pellock, G.C. Walker, P.S. Stewart, G.A. O'Toole, A genetic basis for Pseudomonas aeruginosa biofilm antibiotic resistance, Nature. 426 (6964) (2003) 306–310.
[5] WHO, WHO Publishes List of Bacteria for Which New Antibiotics Are Urgently Needed. Geneva: World Health Organization, 2017.
[6] D. Davies, Understanding biofilm resistance to antibacterial agents, Nat. Rev. Drug Discov. 2 (2) (2003) 114–122.
[7] K. Rupel, L. Zupin, G. Ottaviani, I. Bertani, V. Martinelli, D. Porrelli, S. Vodret, R. Vuerich, D. Passos da Silva, R. Bussani, S. Crovella, M. Parsek, V. Venturi, R. Di Lenarda, M. Biasotto, S. Zacchigna, Blue laser light inhibits biofilm formation in vitro and in vivo by inducing oxidative stress, Npj Biofilms Microbiomes. 5 (2019) 29, https://doi.org/10.1038/s41522-019-0102-9.
[8] V. Kochkodan, N. Hilal, A comprehensive review on surface modified polymer membranes for biofouling mitigation, Desalination. 356 (2015) 187–207.
[9] N. Bazrafshan, M. Dadashi Firouzjaei, M. Elliott, A. Moradkhani, A. Rahimpour, Preparation and modification of low-fouling ultrafiltration membranes for cheese whey treatment by membrane bioreactor, Case Stud. Chem. Environ. Eng. 4 (2021) 100137, https://doi.org/10.1016/j.cscee.2021.100137.
[10] H.-C. Flemming, G. Schaule, T. Griebe, J. Schmitt, A. Tamachkiarowa, Biofouling—the Achilles heel of membrane processes, Desalination. 113 (2-3) (1997) 215–225, https://doi.org/10.1016/S0011-9164(97)00132-X.
[11] M.D. Firouzjaei, S.F. Seyedpour, S.A. Aktij, M. Giagnorio, N. Bazrafshan, A. Mollahosseini, F. Samadi, S. Ahmadalipour, F.D. Firouzjaei, M.R. Esfahani, Recent advances in functionalized polymer membranes for biofouling control and mitigation in forward osmosis, J. Memb. Sci. 596 (2020), 117604.
[12] M. Elimelech, W.A. Phillip, The future of seawater desalination: energy, technology, and the environment, Science (80-.) 333 (2011) 712–717.
[13] B. Meyer, Approaches to prevention, removal and killing of biofilms, Int. Biodeterior. Biodegradation. 51 (4) (2003) 249–253.
[14] H.J. de Vries, F. Beyer, M. Jarzembowska, J. Lipińska, P. van den Brink, A. Zwijnenburg, P.H.A. Timmers, A.J.M. Stams, C.M. Plugge, Isolation and characterization of Sphingomonadaceae from fouled membranes, Npj Biofilms Microbiomes. 5 (2019) 1–9.
[15] B. Khorshidi, I. Biswas, T. Ghosh, T. Thundat, M. Sadrzadeh, Robust fabrication of thin film polyamide-TiO 2 nanocomposite membranes with enhanced thermal stability and anti-biofouling propensity, Sci. Rep. 8 (2018) 1–10.
[16] M. Herzberg, M. Elimelech, Biofouling of reverse osmosis membranes: Role of biofilm-enhanced osmotic pressure, J. Memb. Sci. 295 (1-2) (2007) 11–20, https://doi.org/10.1016/j.memsci.2007.02.024.
[17] S.F. Seyedpour, M. Dadashi Firouzjaei, A. Rahimpour, E. Zolghadr, A. Arabi Shamsabadi, P. Das, F. Akbari Afkhami, M. Sadrzadeh, A. Tiraferri, M.A. Elliott, Toward Sustainable Tackling of Biofouling Implications and Improved Performance of TFC FO Membranes Modified by Ag-MOFs Nanorods, ACS Appl, Mater. Interfaces. 8 (2020) 7588–7599.
[18] C. Liu, A.F. Faria, J. Ma, M. Elimelech, Mitigation of biofilm development on thin-film composite membranes functionalized with zwitterionic polymers and silver nanoparticles, Environ. Sci. Technol. 51 (1) (2017) 182–191.
[19] M. Pejman, M. Dadashi Firouzjaei, S. Aghapour Aktij, P. Das, E. Zolghadr, H. Jafarian, A. Arabi Shamsabadi, M. Elliott, M. Sadrzadeh, M. Sangermano, A. Rahimpour, A. Tiraferri, In Situ Ag-MOF Growth on Pre-Grafted Zwitterions Imparts Outstanding Antifouling Properties to Forward Osmosis Membranes, ACS Appl. Mater. Interfaces. 12 (32) (2020) 36287–36300.
[20] M.D. Firouzjaei, A.A. Shamsabadi, S.A. Aktij, S.F. Seyedpour, M. Sharifian Gh., A. Rahimpour, M.R. Esfahani, M. Ulbricht, M. Soroush, Exploiting synergetic effects of graphene oxide and a silver-based metal–organic framework to enhance antifouling and anti-biofouling properties of thin-film nanocomposite membranes, ACS Appl. Mater. Interfaces. 10 (49) (2018) 42967–42978.
[21] H. Erer, O.Z. Yeşilel, C. Darcan, O. Büyükgüngör, Synthesis, spectroscopic, thermal studies, antimicrobial activities and crystal structures of Co (II), Ni (II), Cu (II) and Zn (II)-orotate complexes with 2-methylimidazole, Polyhedron. 28 (14) (2009) 3087–3093.
[22] S.F. Seyedpour, A. Arabi Shamsabadi, S. Khoshhal Salestan, M. Dadashi Firouzjaei, M. Sharifian Gh, A. Rahimpour, F. Akbari Afkhami, M.R. Shirzad Kebria, M. A. Elliott, A. Tiraferri, M. Sangermano, M.R. Esfahani, M. Soroush, Tailoring the Biocidal Activity of Novel Silver-Based Metal Azolate Frameworks, ACS Sustain. Chem. Eng. 8 (20) (2020) 7588–7599.
[23] A. Rahimpour, S.F. Seyedpour, S. Aghapour Aktij, M. Dadashi Firouzjaei, A. Zirehpour, A. Arabi Shamsabadi, S. Khoshhal Salestan, M. Jabbari, M. Soroush, Simultaneous Improvement of Antimicrobial, Antifouling, and Transport Properties of Forward Osmosis Membranes with Immobilized Highly-Compatible

Polyrhodanine Nanoparticles, Environ. Sci. Technol. 52 (9) (2018) 5246–5258, https://doi.org/10.1021/acs.est.8b0080410.1021/acs.est.8b00804.s001.
[24] J. Yin, G. Zhu, B. Deng, Graphene oxide (GO) enhanced polyamide (PA) thin-film nanocomposite (TFN) membrane for water purification, Desalination. 379 (2016) 93–101, https://doi.org/10.1016/j.desal.2015.11.001.
[25] B. Khorshidi, T. Thundat, B.A. Fleck, M. Sadrzadeh, Thin film composite polyamide membranes: parametric study on the influence of synthesis conditions, RSC Adv. 5 (2015) 54985–54997.
[26] X. Wei, Z. Wang, J. Wang, S. Wang, A novel method of surface modification to polysulfone ultrafiltration membrane by preadsorption of citric acid or sodium bisulfite, Memb. Water Treat. 3 (1) (2012) 35–49.
[27] M.I. Baig, P.G. Ingole, W.K. Choi, J.-D. Jeon, B. Jang, J.H. Moon, H.K. Lee, Synthesis and characterization of thin film nanocomposite membranes incorporated with surface functionalized Silicon nanoparticles for improved water vapor permeation performance, Chem. Eng. J. 308 (2017) 27–39.
[28] B. Das, S.K. Dash, D. Mandal, T. Ghosh, S. Chattopadhyay, S. Tripathy, S. Das, S. K. Dey, D. Das, S. Roy, Green synthesized silver nanoparticles destroy multidrug resistant bacteria via reactive oxygen species mediated membrane damage, Arab. J. Chem. 10 (6) (2017) 862–876.
[29] Y. Zhang, Y. Jia, Li'an Hou, Synthesis of zeolitic imidazolate framework-8 on polyester fiber for PM 2.5 removal, RSC Adv. 8 (55) (2018) 31471–31477.
[30] L. Sarango, J. Benito, I. Gascón, B. Zornoza, J. Coronas, Homogeneous thin coatings of zeolitic imidazolate frameworks prepared on quartz crystal sensors for CO2 adsorption, Microporous Mesoporous Mater. 272 (2018) 44–52.
[31] D. Huang, Q. Xin, Y. Ni, Y. Shuai, S. Wang, Y. Li, H. Ye, L. Lin, X. Ding, Y. Zhang, Synergistic effects of zeolite imidazole framework@ graphene oxide composites in humidified mixed matrix membranes on CO 2 separation, RSC Adv. 8 (11) (2018) 6099–6109.
[32] C.D. Wagner, A. V Naumkin, A. Kraut-Vass, J.W. Allison, C.J. Powell, J.R. Rumble Jr, NIST X-ray Photoelectron Spectroscopy Database, NIST Standard Reference Database 20, Version 3.4 (Web Version), U. S. Dep. Commer. (2003).
[33] Z. Liu, J. Ou, H. Wang, X. You, M. Ye, Synthesis and characterization of hydrazide-linked and amide-linked organic polymers, ACS Appl. Mater. Interfaces. 8 (46) (2016) 32060–32067.
[34] Y. Sun, J. Hu, S. An, Q. Zhang, Y. Guo, D. Song, Q. Shang, Selective esterification of glycerol with acetic acid or lauric acid over rod-like carbon-based sulfonic acid functionalized ionic liquids, Fuel. 207 (2017) 136–145.
[35] S. Kim, Y.S. Yun, Y.E. Choi, Development of waste biomass based sorbent for removal of cyanotoxin microcystin-LR from aqueous phases, Bioresour. Technol. 247 (2018) 690–696, https://doi.org/10.1016/j.biortech.2017.09.164.
[36] H. Zarrok, A. Zarrouk, B. Hammouti, R. Salghi, C. Jama, F. Bentiss, Corrosion control of carbon steel in phosphoric acid by purpald–weight loss, electrochemical and XPS studies, Corros. Sci. 64 (2012) 243–252.
[37] Z. Cao, Y. Tang, H. Cang, J. Xu, G. Lu, W. Jing, Novel benzimidazole derivatives as corrosion inhibitors of mild steel in the acidic media. Part II: Theoretical studies, Corros. Sci. 83 (2014) 292–298.
[38] A.C. Dhayagude, N. Maiti, A.K. Debnath, S.S. Joshi, S. Kapoor, Metal nanoparticle catalyzed charge rearrangement in selenourea probed by surface-enhanced Raman scattering, RSC Adv. 6 (21) (2016) 17405–17414.
[39] J. Benavente, M.I. Vázquez, Effect of age and chemical treatments on characteristic parameters for active and porous sublayers of polymeric composite membranes, J. Colloid Interface Sci. 273 (2) (2004) 547–555.
[40] M. Sadeghi, A. Arabi Shamsabadi, A. Ronasi, A.P. Isfahani, M. Dinari, M. Soroush, Engineering the dispersion of nanoparticles in polyurethane membranes to control membrane physical and transport properties, Chem. Eng. Sci. 192 (2018) 688–698.
[41] X. Song, Q. Zhou, T. Zhang, H. Xu, Z. Wang, Pressure-assisted preparation of graphene oxide quantum dot-incorporated reverse osmosis membranes: antifouling and chlorine resistance potentials, J. Mater. Chem. A. 4 (43) (2016) 16896–16905, https://doi.org/10.1039/C6TA06636D.
[42] S. Xia, L. Yao, Y.u. Zhao, N. Li, Y.i. Zheng, Preparation of graphene oxide modified polyamide thin film composite membranes with improved hydrophilicity for natural organic matter removal, Chem. Eng. J. 280 (2015) 720–727.
[43] V. Vatanpour, S.S. Madaeni, L. Rajabi, S. Zinadini, A.A. Derakhshan, Boehmite nanoparticles as a new nanofiller for preparation of antifouling mixed matrix membranes, J. Memb. Sci. 401-402 (2012) 132–143.
[44] C.H. Lau, T.-S. Chung, Effects of Si–O–Si agglomerations on CO2 transport and separation properties of sol-derived nanohybrid membranes, Macromolecules. 44 (15) (2011) 6057–6066.
[45] M. Asadollahi, D. Bastani, S.A. Musavi, Enhancement of surface properties and performance of reverse osmosis membranes after surface modification: a review, Desalination. 420 (2017) 330–383.
[46] A. Zirehpour, A. Rahimpour, S. Khoshhal, M.D. Firouzjaei, A.A. Ghoreyshi, The impact of MOF feasibility to improve the desalination performance and antifouling properties of FO membranes, RSC Adv. 6 (74) (2016) 70174–70185, https://doi.org/10.1039/C6RA14591D.
[47] A.E. Childress, M. Elimelech, Effect of solution chemistry on the surface charge of polymeric reverse osmosis and nanofiltration membranes, J. Memb. Sci. 119 (2) (1996) 253–268.
[48] M.D. Firouzjaei, F.A. Afkhami, M.R. Esfahani, C.H. Turner, S. Nejati, Experimental and molecular dynamics study on dye removal from water by a graphene oxide-copper-metal organic framework nanocomposite, J. Water Process Eng. 34 (2020), 101180.
[49] C.-J. Yeh, B.-L. Hsi, W. Page Faulk, Propidium Iodide as a Nuclear Marker in Immunofluorescence. II. Use with Cellular Identification and Viability Studies, J. Immunol. Methods. 43 (3) (1981) 269–275, https://doi.org/10.1016/0022-1759(81)90174-5.
[50] K. Zheng, M.I. Setyawati, D.T. Leong, J. Xie, Antimicrobial Gold Nanoclusters, ACS Nano. 11 (7) (2017) 6904–6910.
[51] L. Tan, J. Li, X. Liu, Z. Cui, X. Yang, K.W.K. Yeung, H. Pan, Y. Zheng, X. Wang, S. Wu, In Situ Disinfection through Photoinspired Radical Oxygen Species Storage and Thermal-Triggered Release from Black Phosphorous with Strengthened Chemical Stability, Small. 14 (2018) 1703197.
[52] R. Sommer, S. Wagner, K. Rox, A. Varrot, D. Hauck, E.-C. Wamhoff, J. Schreiber, T. Ryckmans, T. Brunner, C. Rademacher, R.W. Hartmann, M. Brönstrup, A. Imberty, A. Titz, Glycomimetic, orally bioavailable LecB inhibitors block biofilm formation of Pseudomonas aeruginosa, J. Am. Chem. Soc. 140 (7) (2018) 2537–2545.
[53] Mehdi Pejman, Mostafa Dadashi Firouzjaei, Sadegh Aghapour Aktij, Parnab Das, Ehsan Zolghadr, Hesam Jafarian, Ahmad Arabi Shamsabadi, Mark Elliott, Milad Rabbani Esfahani, Marco Sangermano, Mohtada Sadrzadeh, Evan K. Wujcik, Ahmad Rahimpour, Alberto Tiraferri, Improved antifouling and antibacterial properties of forward osmosis membranes through surface modification with zwitterions and silver-based metal organic frameworks, J. Memb. Sci. 611 (2020) 118352, https://doi.org/10.1016/j.memsci.2020.118352.
[54] M. Pejman, M. Dadashi Firouzjaei, S. Aghapour Aktij, P. Das, E. Zolghadr, H. Jafarian, A. Arabi Shamsabadi, M.A. Elliott, M. Sadrzadeh, M. Sangermano, A. Rahimpour, A. Tiraferri, In-Situ Ag-MOFs Growth on Pre-Grafted Zwitterions Imparts Outstanding Antifouling Properties to Forward Osmosis Membranes, ACS Appl, Mater. Interfaces. (2020), https://doi.org/10.1021/acsami.0c12141.
[55] Robert Dawson, Andrew I. Cooper, Dave J. Adams, Nanoporous organic polymer networks, Prog. Polym. Sci. 37 (4) (2012) 530–563.
[56] Alberto Tiraferri, Ngai Yin Yip, Anthony P. Straub, Santiago Romero-Vargas Castrillon, Menachem Elimelech, A method for the simultaneous determination of transport and structural parameters of forward osmosis membranes, J. Memb. Sci. 444 (2013) 523–538.
[57] D.H.N. Perera, Q. Song, H. Qiblawey, E. Sivaniah, Regulating the aqueous phase monomer balance for flux improvement in polyamide thin film composite membranes, J. Memb. Sci. 487 (2015) 74–82.
[58] M.E.A. Ali, L. Wang, X. Wang, X. Feng, Thin film composite membranes embedded with graphene oxide for water desalination, Desalination. 386 (2016) 67–76, https://doi.org/10.1016/j.desal.2016.02.034.
[59] Saira Bano, Asif Mahmood, Seong-Joong Kim, Kew-Ho Lee, Graphene oxide modified polyamide nanofiltration membrane with improved flux and antifouling properties, J. Mater. Chem. A. 3 (5) (2015) 2065–2071, https://doi.org/10.1039/C4TA03607G.
[60] N.K. Saha, S.V. Joshi, Performance evaluation of thin film composite polyamide nanofiltration membrane with variation in monomer type, J. Memb. Sci. 342 (2009) 60–69, https://doi.org/10.1016/j.memsci.2009.06.025.
[61] William A. Phillip, Jui Shan Yong, Menachem Elimelech, Reverse draw solute permeation in forward osmosis: modeling and experiments, Environ. Sci. Technol. 44 (13) (2010) 5170–5176.
[62] Mary L. Lind, Asim K. Ghosh, Anna Jawor, Xiaofei Huang, William Hou, Yang Yang, Eric M.V. Hoek, Influence of zeolite crystal size on zeolite-polyamide thin film nanocomposite membranes, Langmuir. 25 (17) (2009) 10139–10145.
[63] Mehdi Pejman, Firouzjaei Mostafa Dadashi, Sadegh Aghapour Aktij, Ehsan Zolghadr, Parnab Das, Mark Elliott, Mohtada Sadrzadeh, Marco Sangermano, Ahmad Rahimpour, Tiraferri Alberto, Effective strategy for UV-mediated grafting of biocidal Ag-MOFs on polymeric membranes aimed at enhanced water ultrafiltration, Chem. Eng. J. (2021) 130704.